Environmental Science & Technology Letters

Letter

pubs.acs.org/journal/estlcu

Active Tetrahedral Iron Sites of γ-Fe_2O_3 Catalyzing NO Reduction by NH_3

Weiye Qu,[†] Yaxin Chen,[†] Zhiwei Huang,[†] Jiayi Gao,[†] Meijuan Zhou,[†] Junxiao Chen,[†] Chao Li,[†] Zhen Ma,[†] Jianmin Chen,[†] and Xingfu Tang*[,†,‡]

[†]Institute of Atmospheric Sciences, Shanghai Key Laboratory of Atmospheric Particle Pollution & Prevention (LAP3), Department of Environmental Science & Engineering, Fudan University, Shanghai 200433, China

[‡]Jiangsu Collaborative Innovation Center of Atmospheric Environment and Equipment Technology (CICAEET), Nanjing University of Information Science & Technology, Nanjing 210044, China

Supporting Information

ABSTRACT: Maghemite (γ-Fe_2O_3) with a spinel structure, consisting of tetrahedral Fe^{3+} (Fe^{3+}_{Td}) and octahedral Fe^{3+} (Fe^{3+}_{Oh}) sites, has been intensively investigated as an environmentally benign catalyst for selective catalytic reduction (SCR) of NO_x with NH_3. In most cases, Fe^{3+}_{Oh} sites were regarded as catalytically active sites (CASs). Here we identify the CASs in SCR by substituting Fe^{3+}_{Oh} or Fe^{3+}_{Td} sites of γ-Fe_2O_3 with catalytically inactive Ti^{4+} or Zn^{2+}, respectively. The SCR activity of γ-Fe_2O_3 is preserved after Ti^{4+} doping but drastically decreases when the catalyst is doped with Zn^{2+}, demonstrating that Fe^{3+}_{Td} sites serve as CASs in SCR. Synchrotron X-ray absorption spectra coupled with density functional theory calculations reveal that the transfer of an electron from inactive Fe^{2+} to active Fe^{3+} in the tetrahedral site is easier than that in the octahedral site, making the tetrahedral iron sites active in SCR.

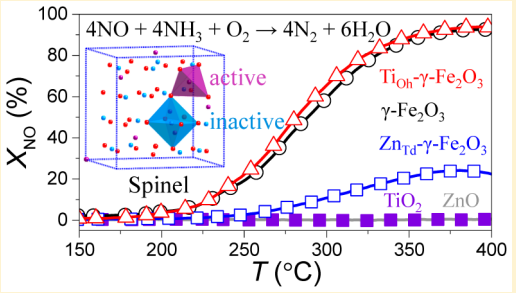

INTRODUCTION

Selective catalytic reduction (SCR) of NO_x with NH_3 is one of the most promising technologies for controlling NO_x emissions that contribute greatly to atmospheric pollution.[1,2] Although V_2O_5-based catalysts have been widely applied for SCR in coal-fired power plants,[3,4] it is necessary to develop vanadium-free SCR catalysts because of the toxicity of vanadium. Fe_2O_3 is an appealing alternative because of its strong resistance to SO_2.[5−8] There are two types of Fe_2O_3, i.e., hematite (α-Fe_2O_3) and maghemite (γ-Fe_2O_3).[9] α-Fe_2O_3 has high thermal stability but shows insufficient activity in the operating temperature window of 300−400 °C. On the contrary, γ-Fe_2O_3 is more active than α-Fe_2O_3 at relatively low temperatures,[10] but γ-Fe_2O_3 transforms into α-Fe_2O_3 above 320 °C,[11] leading to decreased catalytic activity.

An efficient approach to enhancing the thermal stability of γ-Fe_2O_3 is to substitute part Fe^{3+} with other metal ions.[11] To choose desired doping metal ions, identification of catalytically active sites (CASs) of γ-Fe_2O_3 in SCR is one of the important prerequisites. γ-Fe_2O_3 with a spinel structure consists of two types of Fe^{3+}: one-third of Fe^{3+} in the tetrahedral sites (Fe^{3+}_{Td}) and two-thirds of Fe^{3+} in the octahedral sites (Fe^{3+}_{Oh}).[12] It has been overwhelmingly believed that Fe^{3+}_{Oh} sites are CASs for two reasons. (i) The mean length (2.09 Å) of the Fe^{3+}_{Oh}−O bond is greater than that (1.87 Å) of the Fe^{3+}_{Td}−O bond;[5] thus, the former would be more reducible and reactive. (ii) For metal oxide spinels, the octahedral sites are preferentially located at the outermost surface layers as compared with the tetrahedral sites.[13] Even though Ti-doped γ-Fe_2O_3 and Zn-doped γ-Fe_2O_3 have been developed for SCR,[7,14] the local structures of Ti^{4+} and Zn^{2+} were not precisely studied, and the authors of these studies still regarded Fe^{3+}_{Oh} sites as CASs in SCR.

In this work, we identified CASs of γ-Fe_2O_3 in SCR by using a metal ion doping strategy and chose catalytically inactive Ti^{4+} (d^0) and Zn^{2+} (d^{10}) to replace Fe^{3+}_{Oh} and Fe^{3+}_{Td}, respectively. First, the crystal structures of the samples were studied by synchrotron X-ray diffraction (SXRD), and the immediate structures of Ti^{4+} and Zn^{2+} were determined by X-ray absorption near-edge structure (XANES) and extended X-ray absorption fine structure (EXAFS) spectra. Second, the electronic structures of the Fe 3d orbitals were characterized by Fe L_3-edge X-ray absorption spectra coupled with density functional theory calculations. Finally, CASs were identified by correlating the electronic structures of the Fe 3d orbitals with SCR performance. This work clearly shows that Fe^{3+}_{Td} sites are CASs in SCR.

MATERIALS AND METHODS

γ-Fe_2O_3, Zn-γ-Fe_2O_3, and Ti-γ-Fe_2O_3 were prepared by co-precipitation (see details in the Supporting Information). According to the X-ray fluorescence (XRF) spectra (Bruker-AXS S4 Explorer) (Table S1), the molar ratios of Ti to Fe and Zn to Fe are 1:3.3 and 1:3.0, respectively, from which Ti-γ-

Received: April 8, 2017
Revised: May 3, 2017
Accepted: May 5, 2017
Published: May 5, 2017

Downloaded via FUDAN UNIV on November 28, 2018 at 06:18:03 (UTC).
See https://pubs.acs.org/sharingguidelines for options on how to legitimately share published articles.

ACS Publications © 2017 American Chemical Society

DOI: 10.1021/acs.estlett.7b00124
Environ. Sci. Technol. Lett. 2017, 4, 246−250

Fe_2O_3 and Zn-γ-Fe_2O_3 can be roughly formulized as $(Ti_{0.7}Fe_{2.3})_{1-\delta}O_4$ ($0 < \delta < 0.18$) and $(Zn_{0.8}Fe_{2.2})_{1-\delta'}O_4$ ($0 < \delta' < 0.03$), respectively.

Catalytic evaluation, material characterization, and theoretical calculations[15−19] are provided in detail in the Supporting Information.

RESULTS AND DISCUSSION

A high GHSV of 300000 h^{-1} was adopted to differentiate the catalytic activities of γ-Fe_2O_3, Ti-γ-Fe_2O_3, and Zn-γ-Fe_2O_3 in SCR. Figure 1 and Figure S1 show the NO conversions (X_{NO})

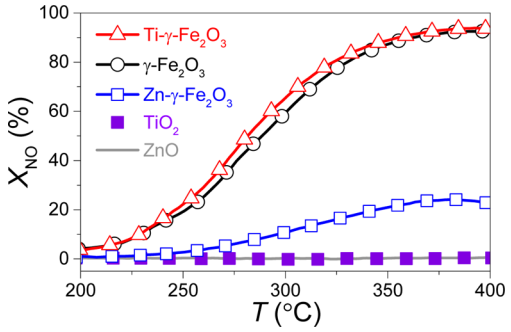

Figure 1. NO conversions (X_{NO}) as a function of temperature (T) over γ-Fe_2O_3, Ti-γ-Fe_2O_3, and Zn-γ-Fe_2O_3 together with TiO_2 and ZnO. Reaction conditions: 500 ppm of NO, 500 ppm of NH_3, 3 vol % O_2, balance N_2, and GHSV of 300000 h^{-1}.

and the selectivity toward N_2 as a function of reaction temperature, respectively. Considering the Zn^{2+} and Ti^{4+} cations cannot usually undergo redox transitions and both TiO_2 and ZnO are inactive in SCR, substituting Ti^{4+} or Zn^{2+} in γ-Fe_2O_3 should not yield extra CASs. As the reaction temperature increases, X_{NO} over pure γ-Fe_2O_3 increases, and X_{NO} reaches ~90% at 400 °C. The specific reaction rates (R) related to surface areas (Table S2) of the catalytic materials are shown in Figure S2. The almost identical X_{NO} (or R) and N_2 selectivity curves can be observed for Ti-γ-Fe_2O_3 except for slight differences in the temperature range of 260−340 °C. In particular, γ-Fe_2O_3 and Ti-γ-Fe_2O_3 almost give the same catalytic activities in the kinetic reaction regime ($X_{NO} < 15\%$), indicating that Ti doping almost has no influence on the catalytic activity of γ-Fe_2O_3. Similarly, Li et al. reported the SCR activity of Ti-γ-Fe_2O_3 is comparable to that over γ-Fe_2O_3.[8,14] Hence, the Fe^{3+} sites substituted with catalytically inactive Ti^{4+} in γ-Fe_2O_3 should not be CASs. On the contrary, Zn-γ-Fe_2O_3 gives a SCR activity significantly lower than that of γ-Fe_2O_3. The catalytic activity of Zn-γ-Fe_2O_3 only slightly increases with reaction temperature, and the X_{NO} values are <25% in the whole temperature window, similar to the previously reported results.[8] This demonstrates that inactive Zn^{2+} ions occupy CASs of γ-Fe_2O_3 in SCR; i.e., the Fe^{3+} sites substituted with catalytically inactive Zn^{2+} in γ-Fe_2O_3 are CASs. These results are further confirmed with varying amounts of doped Ti and Zn (Figure S3).

The reaction kinetics of SCR at a low X_{NO} of <15% were studied. The related Arrhenius plot in terms of the steady-state reaction rate constant (k) is shown in Figure S4, from which the corresponding apparent activation energies (E_a) can be calculated. The average E_a for γ-Fe_2O_3 is ~102 kJ mol^{-1}, equal to that for Ti-γ-Fe_2O_3, indicating that SCR over Ti-γ-Fe_2O_3 and SCR over γ-Fe_2O_3 possibly follow the same reaction mechanism. The calculated pre-exponential factor (Γ) for Ti-γ-Fe_2O_3 (2.5×10^{12} L s^{-1} g^{-1}) approaches that (2.2×10^{12} L s^{-1} g^{-1}) of γ-Fe_2O_3, but it is 5 orders of magnitude larger than that (2.8×10^{7} L s^{-1} g^{-1}) of Zn-γ-Fe_2O_3. The close Γ values imply the same CASs for both γ-Fe_2O_3 and Ti-γ-Fe_2O_3, and the significantly small Γ value for Zn-γ-Fe_2O_3 indicates that the Fe^{3+} sites substituted with Zn^{2+} are CASs of γ-Fe_2O_3.

Figure 2a shows the SXRD patterns. γ-Fe_2O_3 is identified as maghemite with a cubic spinel structure (JPCDS Card No. 39-

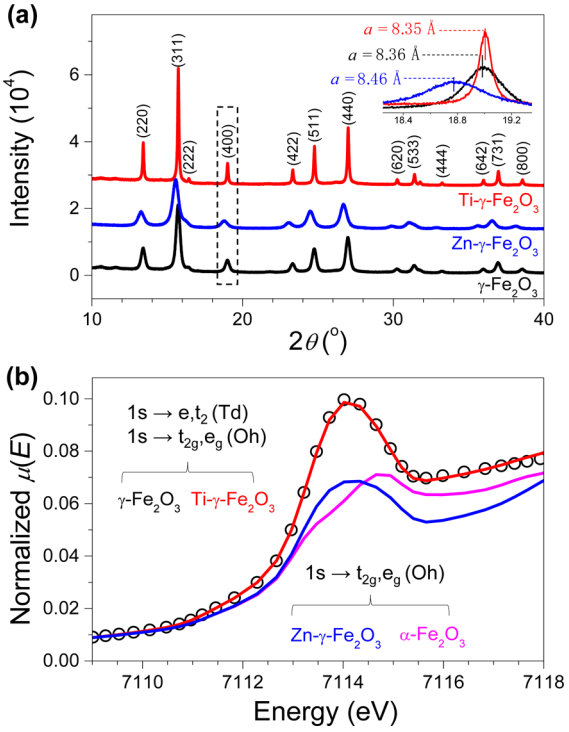

Figure 2. (a) SXRD patterns of γ-Fe_2O_3, Ti-γ-Fe_2O_3, and Zn-γ-Fe_2O_3. (b) Pre-edge XANES spectra of γ-Fe_2O_3 (O), Ti-γ-Fe_2O_3 (red), and Zn-γ-Fe_2O_3 (blue) together with α-Fe_2O_3 (pink) at the Fe K-edge.

1346). The spinel structure is preserved after substitution with Ti^{4+} or Zn^{2+}, and no TiO_2 and ZnO phase appears in the SXRD pattern of Ti-γ-Fe_2O_3 or Zn-γ-Fe_2O_3, respectively. Note that in comparison to those of γ-Fe_2O_3, all the peaks of Zn-γ-Fe_2O_3 distinctly shift to lower Bragg angles, reflecting the substitution of some Fe^{3+} with Zn^{2+} in Zn-γ-Fe_2O_3 by considering that the ionic radius of Zn_{Td}^{2+} (0.60 Å) is larger than that of Fe_{Td}^{3+} (0.49 Å).[20] Similarly, compared to the peaks of γ-Fe_2O_3, all Ti-γ-Fe_2O_3 peaks shift to slightly larger Bragg angles, demonstrating the replacement of some Fe^{3+} with Ti^{4+} due to the ionic radius of Ti_{Oh}^{4+} (0.61 Å) being slightly smaller than that of Fe_{Oh}^{3+} (0.65 Å). Furthermore, the related changes in the lattice parameters calculated from the (400) peaks also indicate the successful substitution of Fe^{3+} with Ti^{4+} or Zn^{2+} (inset of Figure 2a).

The immediate structures of doped Ti^{4+} and Zn^{2+} were determined by XANES and EXAFS. The pre-edge features of the Fe K-edge XANES spectra are sensitive to the local geometrical structures of iron centers.[21] Figure 2b shows the pre-edge XANES spectra of γ-Fe_2O_3, Ti-γ-Fe_2O_3, and Zn-γ-Fe_2O_3 at the Fe K-edge together with a "standard" α-Fe_2O_3 comprising only octahedral FeO_6 structure. A relatively intense pre-edge peak appears in the XANES spectrum of γ-Fe_2O_3, attributed to the 1s → 3d (e, t_2) dipole-allowed transition in

DOI: 10.1021/acs.estlett.7b00124
Environ. Sci. Technol. Lett. 2017, 4, 246−250

Fe^{3+}_{Td} centers and the weak 1s → 3d (t_{2g}, e_g) quadrupole-allowed transition in Fe^{3+}_{Oh} centers, but the 1s → 3d (t_{2g}, e_g) dipole transition is symmetrically forbidden for Fe^{3+}_{Oh} centers.[21] After Ti^{4+} doping, the intensity of the pre-edge peak of Ti-γ-Fe_2O_3 remains unchanged, indicating that Ti^{4+} did not replace Fe^{3+}_{Td} sites of γ-Fe_2O_3. According to the SXRD data and the EXAFS spectrum of Ti-γ-Fe_2O_3 at the Ti *K*-edge (Figure S5), it is convincing to deduce that Ti^{4+} ions occupy Fe^{3+}_{Oh} sites of spinel γ-Fe_2O_3.[22] Note that the intensity of the pre-edge peak at the Fe *K*-edge apparently decreases in the XANES spectrum of Zn-γ-Fe_2O_3, and the normalized absorption coefficient (μ) is ~0.07, the same as that of α-Fe_2O_3 comprising only Fe^{3+}_{Oh}. This is strong evidence that the Fe^{3+} sites substituted with Zn^{2+} are Fe^{3+}_{Td} sites in γ-Fe_2O_3, consistent with the fact that Zn^{2+} ions energetically favorably occupy the tetrahedral sites of spinel structures.[23]

EXAFS spectra were applied to further probe the substituted sites with Ti^{4+} and Zn^{2+} (Figures S6 and S7). The Fourier transform (FT) amplitudes of the $\chi(R)$ k^3-weighted spectra at the *K*-edge are shown in Figure 3. The $\chi(R)$ k^3-weighted FT

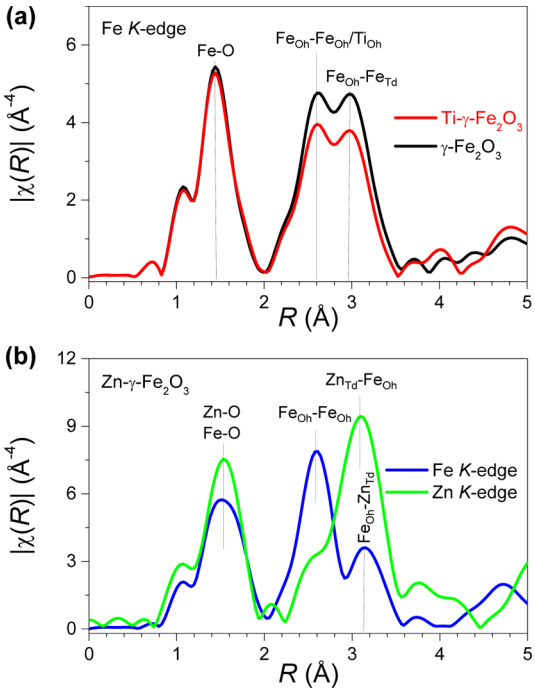

Figure 3. $\chi(R)$ k^3-weighted FT EXAFS spectra of (a) γ-Fe_2O_3 and Ti-γ-Fe_2O_3 at the Fe *K*-edge and (b) Zn-γ-Fe_2O_3 at the Fe and Zn *K*-edges.

EXAFS spectrum of Ti-γ-Fe_2O_3 at the Fe *K*-edge is similar to that of γ-Fe_2O_3, except that the decreases in intensity in the second and third shells of Ti-γ-Fe_2O_3 are observed. The first shell can be attributed to the contribution from the Fe−O bonds with a bond length of ~1.97 Å (Table S3),[22] in line with the average Fe−O bond length (~2.00 Å) in Fe^{3+}_{Td} and Fe^{3+}_{Oh} sites in γ-Fe_2O_3.[24] The second shell is ascribed to the Fe_{Oh}−Fe_{Oh} and Fe_{Oh}−Ti_{Oh} interatomic distances, and the third shell should be assigned to the Fe_{Td}−Fe_{Oh} interatomic distance, which also covers the scattering paths of Fe_{Td} to Ti_{Oh} for Ti-γ-Fe_2O_3. These amplitudes at the second and third shells are weaker than the corresponding amplitude of γ-Fe_2O_3, largely because the atomic number of Ti is smaller than that of Fe.

The three similar shells appear in the FT EXAFS spectrum at the Fe *K*-edge of Zn-γ-Fe_2O_3. The attributions of the first and second shells are shown in Figure 3b, and the amplitude of the third shell is much weaker than the corresponding amplitude of γ-Fe_2O_3, attributed to the interatomic distance between Fe_{Oh} and Zn in the tetrahedral sites. To further substantiate the Zn^{2+} position, we also recorded the FT EXAFS spectrum of Zn-γ-Fe_2O_3 at the Zn *K*-edge (also shown in Figure 3b). The absence of ~3.0 Å interatomic distances demonstrates that Zn^{2+} ions are not located at the octahedral sites of spinel.[22] A combination of the SXRD data with the XANES and EXAFS spectra reveals that Ti^{4+} and Zn^{2+} substituted for the octahedral and tetrahedral sites of spinel γ-Fe_2O_3, respectively.

As shown in Figure 1, the catalytic performance of γ-Fe_2O_3 remains almost preserved after Fe^{3+}_{Oh} sites are substituted with catalytically inactive Ti^{4+}, but γ-Fe_2O_3 loses activity after Fe^{3+}_{Td} sites are substituted with Zn^{2+}, indicating that Fe^{3+}_{Td} sites are CASs in SCR rather than Fe^{3+}_{Oh} sites. Redox cycles are often involved in SCR regardless of the reaction mechanisms (Eley−Rideal and Langmuir−Hinshelwood models),[14,25] and the Fe^{3+} ↔ Fe^{2+} redox cycles occurring during the SCR process are intimately associated with the catalytic activity. Generally, Fe^{3+} sites are responsible for NH_3 oxidation in SCR,[5−8] concomitant with Fe^{3+} → Fe^{2+} transfer, and the subsequently produced Fe^{2+} sites are oxidized to Fe^{3+} by O_2 to finish the redox cycle. The Fe^{3+} → Fe^{2+} transfer is relatively easy because Fe^{3+} has strong oxidative ability, and the Fe^{2+} → Fe^{3+} transfer depends on coordinative configurations of iron ions. Ponec et al. used the isotopic exchange reaction of oxygen to investigate the interactions of Fe_2O_3 (it should be α-Fe_2O_3 with only Fe^{3+}_{Oh} because of an extremely high melting point) with $^{18}O_2$ and found that the E_a value for $^{18}O_2(g) + 2^{16}O_s \rightarrow {}^{16}O_2(g) + 2^{18}O_s$ [where $O_2(g)$ and O_s represent gaseous O_2 and surface lattice oxygen of Fe_2O_3, respectively] is very high, i.e., ~130 kJ mol^{-1} (~1.4 eV per Fe^{3+}_{Oh}) even at 400−500 °C, although the Fe−O bond energy is only 65.7 kJ mol^{-1}.[26] This suggests that the activation energy to realize Fe^{2+}_{Oh} → Fe^{3+}_{Oh} transfer should be higher than the activation energy (~1.1 eV) of SCR over γ-Fe_2O_3 in Figure S4.

To investigate the sustainability of the Fe^{3+} ↔ Fe^{2+} redox cycles at the tetrahedral sites, we collected Fe L_3-edge X-ray absorption spectra (Figure 4a). According to the O_h symmetry of Fe and the crystal-field theory, two peaks in the Fe L_3-edge X-ray absorption spectra of γ-Fe_2O_3, Ti-γ-Fe_2O_3, and Zn-γ-Fe_2O_3 can be assigned to the $2p_{3/2}$ → 3d (t_{2g}, e_g) transitions with an octahedral ligand-field splitting energy (Δ_{Oh}) of ~1.6 eV.[22] The high-spin electron configurations of Fe^{3+}_{Oh} and Fe^{2+}_{Oh} are $t_{2g}^3e_g^2$ and $t_{2g}^4e_g^2$, respectively, and thus, the unoccupied states of the t_{2g} orbitals of Fe^{3+}_{Oh} outnumber those of Fe^{2+}_{Oh}. As a consequence, the unoccupied states of the t_{2g} orbitals are positively proportional to their corresponding intensity in the Fe L_3-edge X-ray absorption spectra. Hence, a ratio (λ) of t_{2g} to e_g in intensity in the Fe L_3-edge X-ray absorption spectrum can be used to determine the oxidation states of Fe_{Oh}.[27] The λ value becomes smaller after Ti^{4+} substitutes for Fe^{3+}_{Oh} in γ-Fe_2O_3, concomitant with the Fe^{3+} → Fe^{2+} transfer in another octahedral site rather than that in the tetrahedral site. This clearly demonstrates that $Fe^{2+}(t_{2g}^4e_g^2)$ is more stable in the octahedral site than in the tetrahedral site; i.e., the propensity of Fe^{2+}_{Td} to be oxidized to Fe^{3+}_{Td} should be higher than that of Fe^{2+}_{Oh} to Fe^{3+}_{Oh}. The λ values for Zn-γ-Fe_2O_3 and γ-Fe_2O_3 are equal to each other, indicating that the $Fe^{3+}_{Oh}(t_{2g}^3e_g^2)$ electron configuration with a Δ_{Oh} value of ~1.6

DOI: 10.1021/acs.estlett.7b00124
Environ. Sci. Technol. Lett. 2017, 4, 246−250

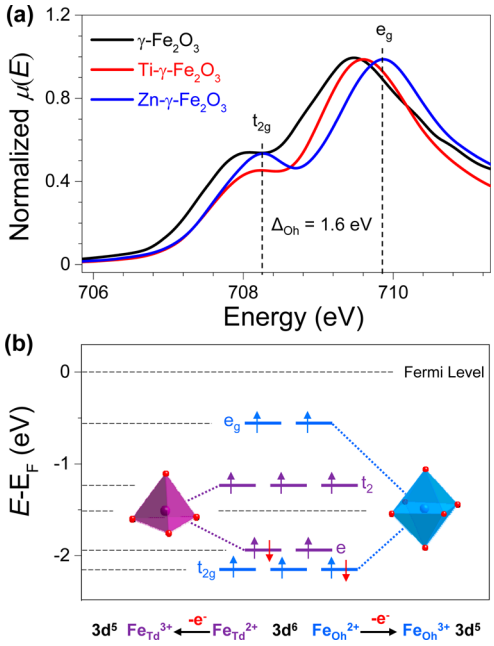

Figure 4. (a) Fe L_3-edge X-ray absorption spectra of γ-Fe_2O_3, Ti-γ-Fe_2O_3, and Zn-γ-Fe_2O_3. (b) Electron configurations of the tetrahedral and octahedral sites in γ-Fe_2O_3. The inset shows the FeO_4 tetrahedron (purple) and FeO_6 octahedron (blue). Red and blue spheres represent O and Fe, respectively.

eV remains preserved after Zn^{2+} replaces $Fe^{3+}{}_{Td}$ (Figure 4a). Therefore, according to the crystal-field theory, a tetrahedral ligand-field splitting energy (Δ_{Td}) for Fe_{Td} in γ-Fe_2O_3 can be calculated to be ~0.7 eV ($\Delta_{Td} = {}^4/_9\Delta_{Oh} = {}^4/_9 \times 1.6$ eV).

The Fe 3d electronic configurations of γ-Fe_2O_3 are plotted in Figure 4b on the basis of the analyses of the Fe L_3-edge X-ray absorption spectra in Figure 4a described above. We further scale the energy of these orbitals by using the DOS of surface γ-Fe_2O_3(110) planes [the exposed (110) surfaces were observed by transmission electron microscopy in Figure S8], which were calculated by DFT (Figure S9). The Fe 3d centroid is calculated to be approximately −1.52 eV, and both $Fe^{3+}{}_{Oh}$ and $Fe^{3+}{}_{Td}$ are high-spin forms because Δ_{Oh} and Δ_{Td} are smaller than the electron pairing energy.[28] In Figure 4b, the $Fe^{2+}{}_{Td} \rightarrow Fe^{3+}{}_{Td}$ transfer by releasing one electron from the $Fe^{2+}{}_{Td}$ e orbital is relatively easier than the $Fe^{2+}{}_{Oh} \rightarrow Fe^{3+}{}_{Oh}$ transfer, indicating that $Fe^{2+}{}_{Td}$ is easily oxidized by O_2 to $Fe^{3+}{}_{Td}$. These results agree fairly with the fact that spinel iron oxides often have inverse spinel structures with Fe^{3+} occupying the tetrahedral sites, consistent with the findings that $Fe^{3+}{}_{Td}$ ions are so active that they preferentially underlie the subsurface layers.[13] Therefore, this work gives a simple and straightforward explanation for why $Fe^{3+}{}_{Td}$ ions of γ-Fe_2O_3 act as CAS in SCR, and it provides a strategy for enhancing the thermal stability to γ-Fe_2O_3 without sacrificing its catalytic performance (Figure S10). Such a redox cycle in γ-Fe_2O_3 may not be unique, because the oxides of Co, Mn, and Ni have similar spinel structures that are often subjected to oxidation−reduction equilibria.[29] Further work is necessary to precisely describe mechanisms of the $Fe^{3+} \leftrightarrow Fe^{2+}$ redox cycles in practical SCR.

■ ASSOCIATED CONTENT

Supporting Information

The Supporting Information is available free of charge on the ACS Publications website at DOI: 10.1021/acs.estlett.7b00124.

Some related tables and figures (PDF)

■ AUTHOR INFORMATION

Corresponding Author

*Telephone: +86-21-65642997. Fax: +86-21-65643597. E-mail: tangxf@fudan.edu.cn.

ORCID

Xingfu Tang: 0000-0002-0746-1294

Notes

The authors declare no competing financial interest.

■ ACKNOWLEDGMENTS

This work was financially supported by the NSFC (21477023) and the STCSM (14JC1400400). The SXRD patterns and X-ray absorption spectra covering XANES and EXAFS spectra were measured at the SSRF and BSRF.

■ REFERENCES

(1) Busca, G.; Lietti, L.; Ramis, G.; Berti, F. Chemical and mechanistic aspects of the selective catalytic reduction of NO_x by ammonia over oxide catalysts: A review. *Appl. Catal., B* **1998**, *18* (1−2), 1−36.

(2) Malakoff, D. A. Nitrogen oxide pollution may spark seeds' growth. *Science* **1997**, *276*, 1199−1199.

(3) Lietti, L.; Nova, I.; Ramis, G.; Dall'Acqua, L.; Busca, G.; Giamello, E.; Forzatti, P.; Bregani, F. Characterization and reactivity of V_2O_5-MoO_3/TiO_2 De-NO_x SCR catalysts. *J. Catal.* **1999**, *187* (2), 419−435.

(4) Janssen, F. J. J. G.; van den Kerkhof, F. M. G.; Bosch, H.; Ross, J. R. H. Mechanism of the reaction of nitric oxide, ammonia, and oxygen over vanadia catalysts. 1. The role of oxygen studied by way of isotopic transients under dilute conditions. *J. Phys. Chem.* **1987**, *91* (23), 5921−5927.

(5) Mou, X.; Zhang, B.; Li, Y.; Yao, L.; Wei, X.; Su, D. S.; Shen, W. Rod-shaped Fe_2O_3 as an efficient catalyst for the selective reduction of nitrogen oxide by ammonia. *Angew. Chem., Int. Ed.* **2012**, *51*, 2989−2993.

(6) Long, R. Q.; Yang, R. T. Superior Fe-ZSM-5 catalyst for selective catalytic reduction of nitric oxide by ammonia. *J. Am. Chem. Soc.* **1999**, *121* (23), 5595−5596.

(7) Wang, C.; Yang, S.; Chang, H.; Peng, Y.; Li, J. Structural effects of iron spinel oxides doped with Mn, Co, Ni and Zn on selective catalytic reduction of NO with NH_3. *J. Mol. Catal. A: Chem.* **2013**, *376*, 13−21.

(8) Yang, S.; Liu, C.; Chang, H.; Ma, L.; Qu, Z.; Yan, N.; Wang, C.; Li, J. Improvement of the activity of γ-Fe_2O_3 for the selective catalytic reduction of NO with NH_3 at high temperatures: NO reduction versus NH_3 oxidization. *Ind. Eng. Chem. Res.* **2013**, *52* (16), 5601−5610.

(9) Machala, L.; Tucek, J.; Zboril, R. Polymorphous transformations of nanometric iron (III) oxide: A review. *Chem. Mater.* **2011**, *23* (14), 3255−3272.

(10) Liu, C.; Yang, S.; Ma, L.; Peng, Y.; Hamidreza, A.; Chang, H.; Li, J. Comparison on the performance of α-Fe_2O_3 and γ-Fe_2O_3 for selective catalytic reduction of nitrogen oxides with ammonia. *Catal. Lett.* **2013**, *143* (7), 697−704.

(11) Lai, J.; Shafi, K. V. P. M.; Loos, K.; Ulman, A.; Lee, Y.; Vogt, T.; Estournes, C. Doping γ-Fe_2O_3 nanoparticles with Mn(III) suppresses the transition to the α-Fe_2O_3 structure. *J. Am. Chem. Soc.* **2003**, *125* (38), 11470−11471.

(12) Buxbaum, G.; Pfaff, G. *Industrial inorganic pigments*, 3rd ed.; John Wiley and Sons: Weinheim, Germany, 2005.

(13) Wachs, I. E.; Routray, K. Catalysis science of bulk mixed oxides. *ACS Catal.* **2012**, *2* (6), 1235−1246.

(14) Yang, S.; Li, J.; Wang, C.; Chen, J.; Ma, L.; Chang, H.; Chen, L.; Peng, Y.; Yan, N. Fe−Ti spinel for the selective catalytic reduction of NO with NH_3: Mechanism and structure−activity relationship. *Appl. Catal., B* **2012**, *117−118*, 73−80.

DOI: 10.1021/acs.estlett.7b00124
Environ. Sci. Technol. Lett. 2017, 4, 246−250

(15) Kresse, G.; Furthmuller, J. Efficient iterative schemes for ab initio total-energy calculations using a plane-wave basis set. *Phys. Rev. B: Condens. Matter Mater. Phys.* **1996**, *54* (16), 11169−11186.
(16) Perdew, J. P.; Burke, K.; Ernzerhof, M. Generalized gradient approximation made simple. *Phys. Rev. Lett.* **1996**, *77* (18), 3865−3868.
(17) Perdew, J. P.; Chevary, J. A.; Vosko, S. H.; Jackson, K. A.; Pederson, M. R.; Singh, D. J.; Fiolhais, C. Atoms, molecules, solids, and surfaces: Applications of the generalized gradient approximation for exchange and correlation. *Phys. Rev. B: Condens. Matter Mater. Phys.* **1992**, *46* (11), 6671−6687.
(18) Blöchl, P. E. Projector augmented-wave method. *Phys. Rev. B: Condens. Matter Mater. Phys.* **1994**, *50* (24), 17953−17979.
(19) Kresse, G.; Hafner, J. Ab initio molecular dynamics for liquid metals. *Phys. Rev. B: Condens. Matter Mater. Phys.* **1993**, *47* (1), 558−561.
(20) Shannon, R. D. Revised effective ionic radii and systematic studies of interatomie distances in halides and chaleogenides. *Acta Crystallogr., Sect. A: Cryst. Phys., Diffr., Theor. Gen. Crystallogr.* **1976**, *32* (5), 751−767.
(21) Bordiga, S.; Groppo, E.; Agostini, G.; van Bokhoven, J. A.; Lamberti, C. Reactivity of surface species in heterogeneous catalysts probed by in situ X-ray absorption techniques. *Chem. Rev.* **2013**, *113* (3), 1736−1850.
(22) Millot, N.; Aymes, D.; Bernard, F.; Niepce, J. C.; Traverse, A.; Bourée, F.; Cheng, B. L.; Perriat, P. Particle size dependency of ternary diagrams at the nanometer scale: Evidence of TiO_2 clusters in Fe-based spinels. *J. Phys. Chem. B* **2003**, *107* (24), 5740−5750.
(23) Wang, H. Y.; Hung, S. F.; Chen, H. Y.; Chan, T. S.; Chen, H. M.; Liu, B. In operando identification of geometrical-site-dependent water oxidation activity of spinel Co_3O_4. *J. Am. Chem. Soc.* **2016**, *138* (1), 36−39.
(24) Jørgensen, J. E.; Mosegaard, L.; Thomsen, L. E.; Jensen, T. R.; Hanson, J. C. Formation of γ-Fe_2O_3 nanoparticles and vacancy ordering: An in situ X-ray powder diffraction study. *J. Solid State Chem.* **2007**, *180* (1), 180−185.
(25) Topsoe, N. Y. Mechanism of the selective catalytic reduction of nitric oxide by ammonia elucidated by in situ on-line Fourier transform infrared spectroscopy. *Science* **1994**, *265* (5176), 1217−1219.
(26) Doornkamp, C.; Clement, M.; Ponec, V. The isotopic exchange reaction of oxygen on metal oxides. *J. Catal.* **1999**, *182* (2), 390−399.
(27) Karppinen, M.; Yamauchi, H.; Yasukawa, Y.; Lindén, J.; Chan, T. S.; Liu, R. S.; Chen, J. M. Valence state of iron in the $Sr_2Fe(Mo,W,Ta)O_{6.0}$ double-perovskite system: An Fe *K*-edge and $L_{2,3}$-edge XANES study. *Chem. Mater.* **2003**, *15* (21), 4118−4121.
(28) Parkinson, G. S. Iron oxide surfaces. *Surf. Sci. Rep.* **2016**, *71* (1), 272−365.
(29) Navrotsky, A.; Ma, C.; Lilova, K.; Birkner, N. Nanophase transition metal oxides show large thermodynamically driven shifts in oxidation-reduction equilibria. *Science* **2010**, *330* (6001), 199−201.

DOI: 10.1021/acs.estlett.7b00124
Environ. Sci. Technol. Lett. 2017, 4, 246−250